Proc. Budapest'02 Workshop on
Quark & Hadron Dynamics (2002) 000–000

Budapest'02 Workshop on
Quark & Hadron Dynamics
Budapest, Hungary
March 3–7, 2002

Particle Production in Pb+Pb Collisions at the SPS

H. Ströbele for the NA49 Collaboration

Universität Frankfurt, IKF
D60486 Frankfurt

Abstract. Experiment NA49 at the Cern SPS employes a large acceptance detector to study particle spectra, yields and correlations in nucleus–nucleus, nucleon–nucleus and nucleon-nucleon collisions. Preliminary results on pinon, kaon, Λ and $\overline{\Lambda}$ production in central Pb+Pb collisions at 40, 80 and 158 A·GeV beam energy are shown and compared to measurements at lower and higher energies.

Keywords: multiplicity, pions, kaons, Λ, $\overline{\Lambda}$
PACS: 25.75.+r

1. Introduction

The primary purpose of the heavy ion programme at the CERN SPS is the search for evidence of a transient deconfined state of strongly interacting matter during the early stage of nucleus–nucleus collisions [1]. The formation of quasi-free quarks and gluons, the quark gluon plasma (QGP), and the subsequent transition to a dilute gas of individual hadrons was first suggested using qualitative arguments [2] and later confirmed by quantum chromodynamics (QCD) on the lattice provided the energy density reaches sufficiently high values in an extended volume. The results from the heavy-ion program at CERN in fact indicate that the initial energy density reaches or even exceeds the critical value within the SPS energy range. The search for signals of deconfinement lead to encouraging results which are considered as circumstantial evidence for the creation of a state of deconfined partons[3].

Originally proposed signatures [4] of the QGP were observed in Pb+Pb collisions at the top SPS energy, i.e. J/Ψ suppression, strangeness enhancement, and possibly thermal photons and dileptons. The significance of these signals as QGP signatures has come under renewed scrutiny. Moreover, there is no observational evidence for a sharp phase transition from QGP to hadrons such as phase coexistence [5], critical fluctuations [5,6] or more speculative effects like DCC [7] or parity violation [8].

The NA49 collaboration aims at a complete set of data on p+p, p+A (see other contributions by NA49 to this volume) and A+A data as function of energy (20–158 A·GeV) in an effort to establish excitation functions of hadronic observables. In the end such data will allow to quantify anomalies in the energy and mass dependence of experimental observables and strengthen decisively the arguments for or against the formation of a new state of matter beyond a hot and dense gas of hadrons.

Data on central A+A collisons at 40, 80 and 158 A·GeV have been recorded and analysed. A brief description of the apparatus (section 2) is followed by preliminary results for π, K, Λ and $\bar{\Lambda}$ yields (section 3) and a comparison to model caluclations (section 4).

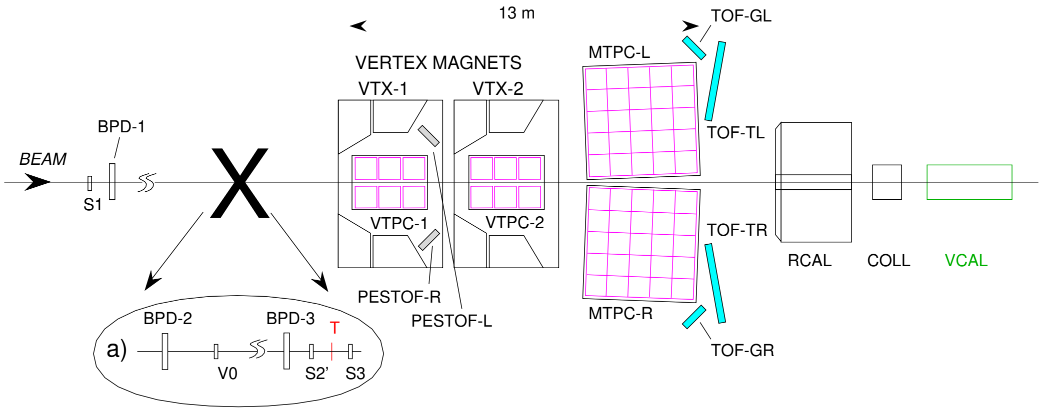

Fig. 1. Schematic layout of the NA49 experiment at the Cern SPS showing beam detectors, superconducting dipole magnets, time projection chambers (VTPC,MTPC), time-of-flight arrays (TOF) and calorimeters (RCAL,VCAL). A thin solid target T is used for A+A collisions (a), which is surrounded by a detector of slow protons (CD) for p+A collsions (c). A liquid H_2 target is employed for p+p collisions (b)

2. The NA49 detector

The NA49 experiment [9] was designed for the investigation of hadron production in the most violent Pb+Pb interactions at the CERN SPS. The main features (Fig.1) are large acceptance precision tracking and particle identification by means of energy loss measurements in the relativistic rise using time projection chambers (TPCs). The first two are located inside superconducting dipole magnets which provide the particle trajectory bending necessary for momentum determination. Charged particles in the forward hemisphere of the reaction are identified from the measurement of their energy loss dE/dx in the TPC gas (accuracy 3 –4 %). At central rapidity the identification is further improved by measurement of the time-of-flight (resolution 60 ps) in two arrays of scintillation counter tiles (TOF-T) and strips (TOF-G). Strange particles are detected via decay topology and invariant mass measurement. The forward calorimeter VCAL measures the energy of the projectile spectators from which one can deduce the impact parameter in A+A collisions.

3. Yields of π, K, Λ and $\bar{\Lambda}$

Raw K^+ and K^- yields were extracted from fits of the distributions of dE/dx and TOF (where available) in narrow bins of rapidity y and transverse momentum p_T. The resulting spectra were then corrected for geometrical acceptance, losses due to in–flight decays and reconstruction efficiency. The latter was determined from embedding simulated tracks into real events and amounted to ≈ 95%. Spectra of π^- mesons were derived from the acceptance corrected negatively charged particle yields in p_T and y (assuming the π mass) by subtracting the estimated contribution of K^-, $\bar{p}$ and the contamination from secondary hadron decays. The ratio π^+/π^- was determined in the region where both dE/dx and TOF are available (0.91, 0.94

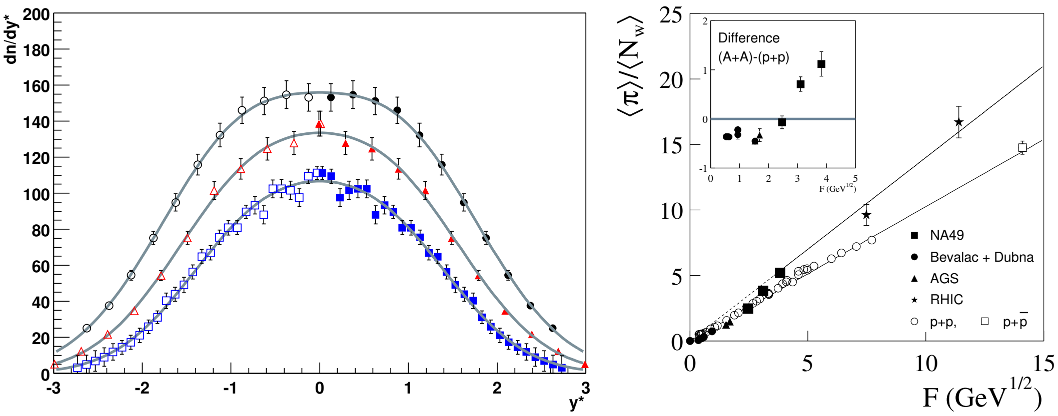

Fig. 2. Left: rapidity distribution of π^- in central Pb+Pb collisons at 40 (squares), 80 (triangles) and 158 (dots) A·GeV. Open symbols show values reflected at $y^\star$=0 (NA49 preliminary). Right: total pion multiplicity $\langle\pi\rangle$ produced per wounded (participant) nucleon versus the Fermi energy variable F ≈ $s_{NN}^{0.25}$ for p+p reactions (open symbols) and central nucleus–nucleus collisions (full symbols). All shown NA49 data are preliminary.

and 0.97 at 40, 80 and 158 A·GeV) and was assumed to be y independent.

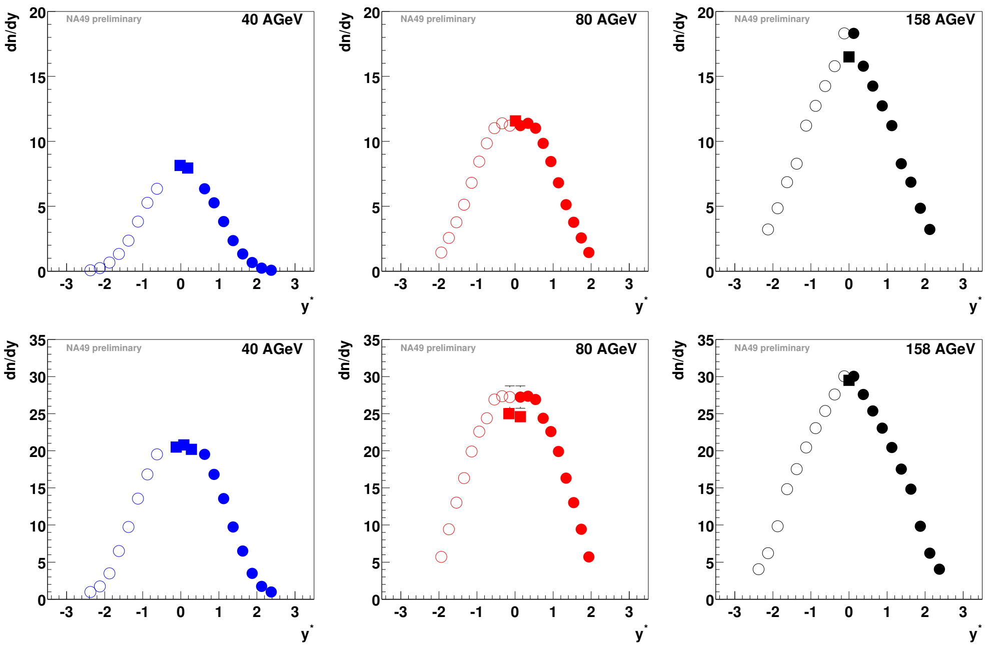

Fig. 3. Rapidity distribution of K^- (top row) and K^+ (bottom row) from dE/dx (circles) and combined dE/dx and TOF (squares) analysis. Open symbols show values reflected at $y^\star$=0. (NA49 preliminary)

The resulting rapidity distributions of π^- are plotted in Fig.2, left. The integrated yields are 312±15, 445±22 and 610±30 at 40, 80 and 158 A·GeV respectively. Pions are the dominant produced particle species and thus their number provides a measure of the entropy in a statistical model description of the reaction. The yield of pions (estimated here as $\langle\pi\rangle = 1.5 \cdot (\langle\pi^-\rangle + \langle\pi^+\rangle)$) divided by the number of wounded nucleons (participants) N_W is shown versus the Fermi energy variable F $\equiv (\sqrt{s} - 2m_N)^{3/4}/\sqrt{s_{NN}}^{1/4} \approx s_{NN}^{1/4}$ in Fig.2, right. While p+p data show a linear rise throughout there is a change for A+A collisions (illustrated more clearly in the inset) in the SPS energy range. Below one finds a regime of slight suppression, above a region of enhancement with a steeper linear rise than for p+p reactions. This steepening has been interpreted as indicating the activation of a large number of partonic degrees of freedom at the onset of deconfinement [10].

Kaons contain about 75% of the $s, \bar{s}$ quarks in the produced hadrons at SPS energies and thus their number indicates the total strangeness content of the final state. The rapidity distributions are displayed in Fig.3 and integrate with small ex-

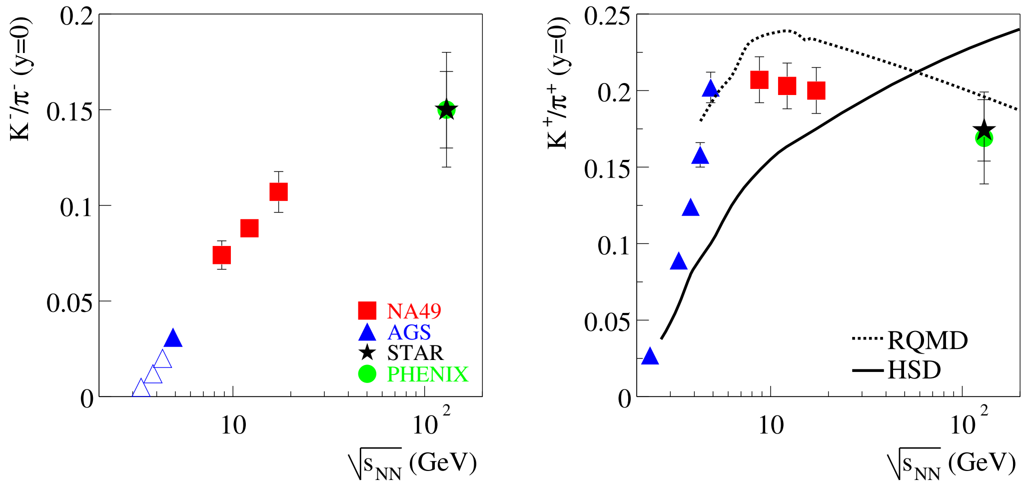

Fig. 4. Midrapidity ratio of K^-/π^- (left) and K^+/π^+ (right) as function of energy from NA49 (squares, preliminary) compared to measurements at lower and higher energies. Predictions of the RQMD [11] (dotted) and HSD [12] (full curve) models are shown.

trapolation to total yields of 18±1, 29±2, 50±5 for K^- and 56±3, 79±5, 95±9 for K^+ at 40, 80, 160 A·GeV respectively. Yields of most particles, of course, increase with energy. Changes in the composition of the produced system are better characterised by particle ratios. Measurements of K^-/π^- and K^+/π^+ at midrapidity from NA49 are plotted versus energy in Fig.4 and compared to results at lower and higher energies. A continuous increase is seen for K^-/π^-. For K^+/π^+ one finds a steeper rise followed by a maximum at the lower end of the SPS energy region and a gradual decrease. Within a reaction scenario based on nucleon–nucleon collisions these features might be attributed to thresholds and the decrease of the baryon density with increasing energy. The ratio K^-/π^- exhibits the threshold of the $K\bar{K}$ production mechanism. The lower mass threshold of associate KY production leads to a steeper rise in K^+/π^+ and the rapidly falling baryon density may result in a compensation of the declining contribution from the KY by the growing contribution from the $K\bar{K}$ production mechanism. However, the continuous increase seen for nucleon–nucleon collisions (e.g. Fig.7, right) does not really support such an interpretation.

The most abundantly produced hyperons are Λ and $\bar{\Lambda}$ for which Fig.5 shows the rapidity distributions. These show a broad shape for Λ reflecting the associate production mechanism and the partially stopped participant nucleon distribution. In contrast the distribution is of narrower Gaussian type for $\bar{\Lambda}$ which are most likely

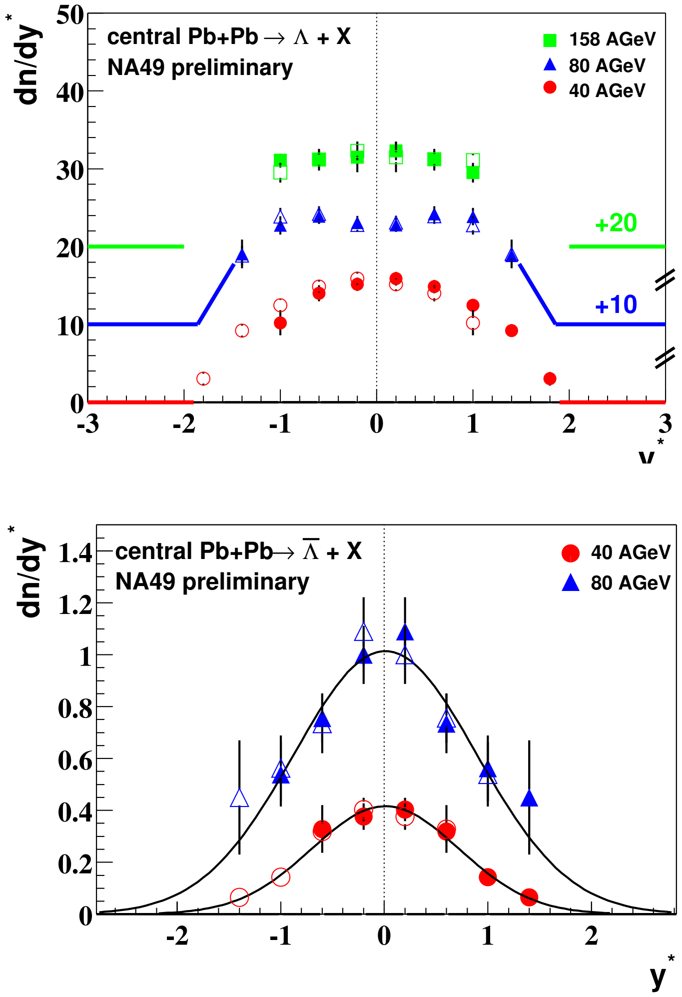

Fig. 5. Rapidity distribution of Λ (left) and $\bar{\Lambda}$ (right). Open symbols show values reflected at $y^{\star}$=0. Λ yields at 80 and 158 A·GeV are displaced vertically by 10 respectively 20 units for clarity. (NA49 preliminary)

produced as members of hyperon–antihyperon ($Y\bar{Y}$) pairs. The ratios $\langle\Lambda\rangle/\langle\pi\rangle$ and $\langle\bar{\Lambda}\rangle/\langle\pi\rangle$ of 4π integrated yields are displayed as a function of energy in Fig.6. One observes a steep threshold rise for the $\langle\Lambda\rangle/\langle\pi\rangle$ ratio followed by a decline which can be mainly attributed to the rapidly decreasing net baryon density. The ratio $\langle\bar{\Lambda}\rangle/\langle\pi\rangle$ exhibits a continuous rise due to the high mass $Y\bar{Y}$ threshold.

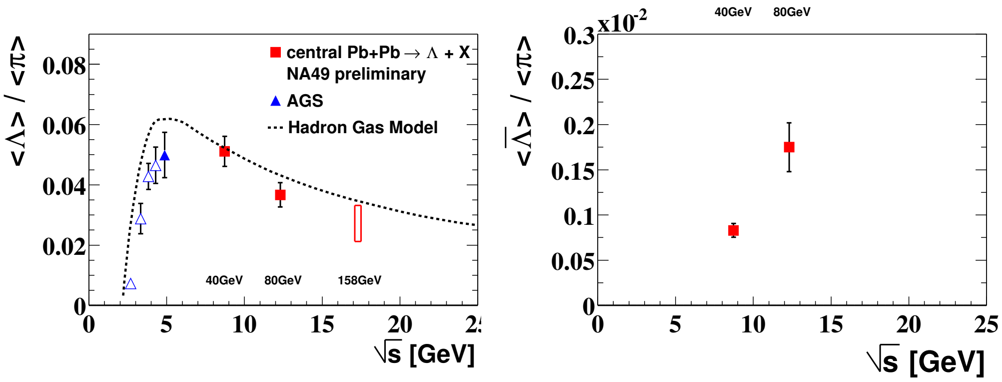

Fig. 6. 4π yield ratios $\langle\Lambda\rangle/\langle\pi\rangle$ (left) and $\langle\bar{\Lambda}\rangle/\langle\pi\rangle$ (right) versus energy from NA49 (squares, preliminary) and lower energy AGS experiments. The dotted line shows a prediction from the extended hadron gas model [13].

4. Comparison to model calculations

Microscopic dynamical and statistical models have been used extensively to describe particle yields in a wide variety of reactions. The first class is often based on string excitation, fusion and hadronisation (e.g. HSD [12], RQMD [11], UrQMD [14]) followed by reinteractions of the formed hadrons (RQMD, UrQMD). As seen from Fig.4 HSD does not reproduce the energy dependence of the midrapidity K^+/π^+ ratio. On the other hand, RQMD correctly predicts the trend, but somewhat overpredicts the ratio in the SPS energy range.

A comparison with the 4π ratio $\langle K^+\rangle/\langle\pi^+\rangle$ is presented in Fig.7 left. Both UrQMD and RQMD get the steep threshold rise. UrQMD values are much too low in the plateau due to an overprediction of pions. RQMD does not follow the drop in the SPS range which is indicated by the measurements. Since antihyperon production rates are small and isospin symmetry approximately holds ($\langle K^+\rangle \approx \langle K^0\rangle$) nearly half of the $\bar{s}$ quarks in the produced hadrons are contained in K^+ mesons. Moreover, strangeness conservation requires $\langle s\rangle = \langle\bar{s}\rangle$. Thus $\langle K^+\rangle$ measures to a good approximation one quarter of all s and $\bar{s}$ quarks in the final state hadrons. The energy dependence of the $\langle K^+\rangle/\langle\pi^+\rangle$ ratio (see Fig.7 left) therefore indicates a maximum in the fraction of strangeness carrying particles in the lower SPS energy range.

Statistical models have been surprisingly successful in describing ratios of particle yields in many types of reactions over a wide energy range. Since the widths of

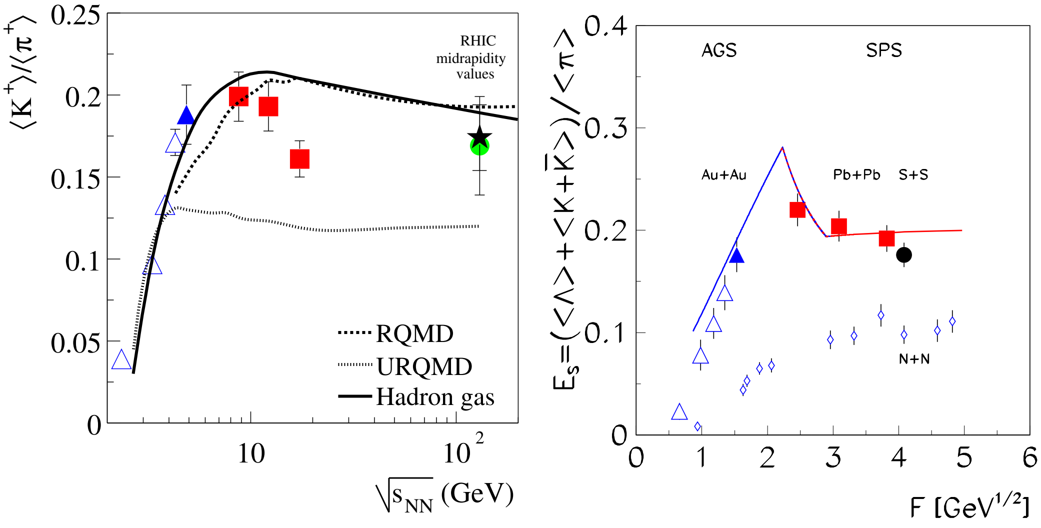

Fig. 7. Left: 4π ratio $\langle K^+\rangle/\langle\pi^+\rangle$ versus energy compared to predictions of the RQMD [11] (dashed), UrQMD [14] (dotted) and extended statistical [13] (solid curve) models. Right: the strangeness content measure E_s versus the Fermi energy variable F$\approx s_{NN}^{0.25}$ compared to the prediction of the statistical model of the early stage [10] (curves).

rapidity distributions depend on particle mass in the SPS energy range and below, the model should preferentially be compared to 4π yields. Fits of this model to NA49 data [15] have indicated that while there is relative hadro–chemical equilibrium in the strange particle sector there seems to be an overall undersaturation with respect to non-strange particle yields. The statistical model as such makes no prediction concerning the energy dependence of particle production. However, it has recently been supplemented [13] by a parameterisation of the energy dependence of its two main parameters, baryochemical potential μ_B and temperature T. Predictions are shown in Fig.7 left for $\langle K^+\rangle/\langle\pi^+\rangle$ and Fig.6 right for $\langle\Lambda\rangle/\langle\pi\rangle$. The trend of the data is well reproduced by this extended statistical model calculation. In detail the decrease in the SPS energy range of both $\langle K^+\rangle/\langle\pi^+\rangle$ and $\langle\Lambda\rangle/\langle\pi\rangle$ and even more so of $\langle\Xi\rangle/\langle\pi\rangle$ (not shown) is not well described.

Predictions have also been published for a statistical model which explicitly assumes a deconfined phase in the early stage above a certain threshold energy [10]. In this model the strangeness to entropy ratio is assumed to be established initially and to persist through the hadronisation stage. A measure of this quantity is the ratio $\mathrm{E}_s = (\langle\Lambda\rangle + \langle K + \bar{K}\rangle)/\langle\pi\rangle$ evaluated from the final hadron multiplicities which is plotted in Fig.7 right. After a rise corresponding to the purely hadronic reaction in the model, one observes a saturation at the a level consistent with the strangeness to entropy ratio expected for an initially deconfined system.

Acknowledgement(s)

This work was supported by the Director, Office of Energy Research, Division of Nuclear Physics of the Office of High Energy and Nuclear Physics of the US Department of Energy (DE-ACO3-76SFOOO98 and DE-FG02-91ER40609), the US National Science Foundation, the Bundesministerium fur Bildung und Forschung, Germany, the Alexander von Humboldt Foundation, the UK Engineering and Physical Sciences Research Council, the Polish State Committee for Scientific Research (5 P03B 13820 and 2 P03B 02418), the Hungarian Scientific Research Foundation (T14920 and T23790), the EC Marie Curie Foundation, and the Polish-German Foundation.

References

1. for review see Proceedings of the 14th International Conference on Ultra–Relativistic Nucleus–Nucleus Collisions, Quark Matter 99, eds.: L. Riccati, M. Masera and E. Vercellin, Nucl. Phys. **A661** (1999) 1c.
2. J. C. Collins and M. J. Perry, Phys. Rev. Lett. **34** (1975) 151.
3. see: http://cern.web.cern.ch/CERN/Announcements/2000/NewStateMatter/
4. review of QGP signatures: J.Harris and B.Müller, Annu. Rev. Nucl. Part. Sci. **46** (1996) 71.
5. C.Hung and E.Shuryak, Phys. Rev. Lett. **75** (1995) 4003.
6. M.Stephanov, K.Rajagopal and E.Shuryak, Phys. Rev. **D60** (1999) 114028.
7. K.Rajagopal and F.Wilczek, Nucl. Phys. **399** (1993) 395; **B404** (1993) 557.
8. D.Kharzeev, R.Pisarski and M.Tytgat, Phys. Rev. Lett. **81** (1998) 512.
9. S.Afanasev et al., Nucl. Inst. Meth. **A430** (1999) 210.
10. M. Gaździcki and M. I. Gorenstein, Acta Phys. Polon. **B30** (1999) 2705, and references therein.
11. F. Wang, H. Liu, H. Sorge, N. Xu and J. Yang, Phys. Rev. **C61** (2000) 064904.
12. W. Cassing, E.L. Bratkovskaya and S. Juchem, Nucl. Phys. **A674** (2000) 249.
13. J. Cleymans and K. Redlich, Phys. Rev. **C60** (1999) 054908, P. Braun-Munzinger et al., Nucl. Phys. **A697** (2002) 902.
14. S. A. Bass et al., Prog. Part. Nucl. Phys. **41** (1998) 225.
15. F.Becattini, M.Gaździcki and J.Sollfrank, Eur. Phys. J. **C5** (1998) 143.